Taguchi optimization of hardness and scratch adhesion strength of multilayer Ti/TiN coatings on Ti- 51 at%Ni alloy deposited via magnetron sputtering technique

Ishiaka Shaibu Arudi [b,****], Esah Hamzah [a,***], Muhammad Azizi Mat Yajid [a], A.R. Bushroa [c,d,**], Shadi M. Munshi [e], M.S. Al-Ashhab [e,f], Mahmoud Z. Ibrahim [c,f,*]

[a] *School of Mechanical Engineering, Universiti Teknologi Malaysia, 81310 Johor, Malaysia*
[b] *Department of Mechanical Engineering, University of Abuja, P.M.B 117 Abuja, Nigeria*
[c] *Department of Mechanical Engineering, Faculty of Engineering, Universiti Malaya, 50603 Kuala Lumpur, Malaysia*
[d] *Advanced Manufacturing and Materials Processing, Department of Mechanical Engineering, Faculty of Engineering, Universiti Malaya, 50603 Kuala Lumpur, Malaysia*
[e] *Department of Mechanical Engineering, College of Engineering and Architecture, Umm Al-Qura University, Mecca 24211, Saudi Arabia*
[f] *Department of Design and Production Engineering, Faculty of Engineering, Ain Shams University, 11517 Cairo, Egypt*

ARTICLE INFO

ABSTRACT

The near equiatomic Ti-51at %Ni alloy has excellent corrosion resistance, strength, shape memory and pseudo-elastic behaviour. However, it is lacking biocompatibility due to the release of hazardous Ni-ions when used as an implant. Thus, this research proposes optimizing the fabrication of multilayer Ti/TiN coating on Ti-51at %Ni alloy using magnetron sputtering. The hardness and adhesion strength are crucial properties to sustain external bearing loads and to ensure the durability of the coating. The process parameters of magnetron sputtering were optimized using Taguchi method. The analysis showed that optimum adhesion strength was obtained at 370 W, 100 °C, 50 V and 5 sccm with respect to DC power, substrate temperature, bias voltage and nitrogen flow, respectively. Whereas, the optimum hardness was obtained at 370 W, 150 °C, 75 V and 5 sccm. The confirmation test evidenced the hardness and adhesion strength improvement by 6.83 % and 10.74 %, respectively. The results of the optimized substrate surface showed a dense and compact growth of the deposited layer with the absence of cracks and pores. Finally, this research demonstrated a promising durable multilayer Ti/TiN coating on Ti-51at %Ni for biomedical applications.

1. Introduction

Titanium-nickel alloys (with Ni 48–51 %) have excellent corrosion resistance besides shape recovery behaviour. The behaviour is due to the shape memory effect and super elasticity making them widely used for biomedical applications [1,2]. Shape memory alloys exhibit good elasticity under stresses and thus return to their original shape [3,4]. Additionally, TiNi alloys may recover a substantial amount of strain (up to 8 %) when heated to ~ 37 °C (human body temperature). This is most likely the same elastic strain of natural bones [5]. Although the excellent corrosion resistance of the Ti–Ni alloy, the release of Ni-ions can cause hypersensitivity in the human body [6–8]. Furthermore, the toxicity effect due to high Ni concentrations can harm bone structures as well as soft tissues [9,10].

To date, there have been several research investigating the biocompatibility of TiNi alloys. Their corrosion resistance and biocompatibility depend mainly on the stability and adherence of a passive TiO_2 film layer on its surface [11,12]. However, this layer is fragile and prone to delamination and failure after implantation [13]. Depositing a coating layer is one of the promising approaches that have been investigated to provide a protective layer as well as induce other functionalities [10,14]. Several coating techniques have been successfully

* Corresponding author. Department of Mechanical Engineering, Faculty of Engineering, Universiti Malaya, 50603 Kuala Lumpur, Malaysia.
*** Corresponding author. School of Mechanical Engineering, Universiti Teknologi Malaysia, 81310 Johor, Malaysia.
** Corresponding author. Department of Mechanical Engineering, Faculty of Engineering, Universiti Malaya, 50603 Kuala Lumpur, Malaysia.
**** Corresponding author. Department of Mechanical Engineering, University of Abuja, P.M.B 117 Abuja, Nigeria.
   E-mail addresses: shuaibu.ishiaka@uniabuja.edu.ng (I.S. Arudi), esah@mail.fkm.utm.my (E. Hamzah), bushroa@um.edu.my (A.R. Bushroa), mahmoud.zakaria@eng.asu.edu.eg (M.Z. Ibrahim).

utilized to develop coating layer on metallic substrates such as physical vapour deposition (PVD) [15,16], thermal spraying [17,18], sol-gel [19,20], and laser cladding [21,22]. The developed coating layers showed significant improvements in hardness, corrosion resistance and biocompatibility [23]. However, delamination is a significant challenge that may occur in the coated implant due to weak adhesion which might negatively affect the efficacy and the work-life of the implant [24,25]. Among these coating techniques, PVD magnetron sputtering offers low processing temperature (200–400 °C) and deposits thin films ranging between 0.5 μm and 3.0 μm [26–28]. Additionally, PVD magnetron sputtering deposits highly adherent and smooth thin films [25,29].

Different coating materials have been considered and investigated for biomedical applications. Bioceramics are one of the most studied materials as coating on Ti alloys. Bioceramics enhance bioactivity, biocompatibility, hardness and wear resistance. However, because their physical properties differ from the substrate, the deposited layer is prone to delamination and cracking. Additionally, they are brittle and resorbable in body [30–32]. Another group of coating materials are bioinert ceramics such as alumina and zirconia [33,34]. However, these bioceramics are degraded and lose their mechanical properties in aquas mediums [35,36].

TiN coating is highly desirable for its high hardness, high resistance to wear and corrosion, and oxidation resistance [37–39]. To address the issue of delamination and other defects that may occur in a deposited biomedical implant in addition to possibility of failure because of residual stresses, Ti is often used as an interlayer between TiN thin film and TiNi substrate which minimizes and relaxes residual stress within the Ti/TiN layer [40–42]. However, careful selection of deposition parameters is crucial to minimize the residual stresses which may fail the deposited thin film [43,44].

The coating of TiN on Ti-alloy based implants is often carried out by PVD magnetron sputtering to increase the adhesion strength and hardness [45]. The process involves the reaction of nitrogen gas and pure Ti to form vapour before deposition [46]. The adhesion strength is influenced by process parameters; substrate temperature, RF power, gas flow rate (Ar, Ar/N_2), DC voltage, and target-to-substrate distance [47]. Despite all the conducted reported research, the best combination parameters for Ti/TiN layer on the Ti-based alloys are still under investigation to optimize the hardness and adhesion strength.

Therefore, this research aims to adapt Taguchi method in analyzing responses (the measured hardness as well as adhesion strength) to achieve the optimum conditions. Taguchi method offers an effective and systematic procedure to parameter optimization through Design of Experiment (DOE), which is a method of the experimental design process with the minimum number of experiments to be carried out to achieve the vital information required through the application of statistical methods. It is considered as the most suitable tool for optimum factor solution with minimal efforts under different variable conditions. Zalnezhad et al. used the method to obtain the best parameters to achieve the best adhesion strength, surface hardness and surface roughness by implementing the method of signal to noise ratio (S/N) analysis [45].

The multilayer Ti/TiN coating was developed utilizing the PVD magnetron sputtering technique. Field-emission electron microscope (FESEM), energy-dispersive X-ray (EDX), and X-ray diffraction (XRD) were used to examine the microstructure, elemental composition and structural phases present within the optimized deposited coating, respectively. The adhesion strength was estimated using a micro-scratch test equipped with an optical microscope. Meanwhile, the hardness of the coating layer was measured by Vickers's microhardness testing machine. The optimized hardness and adhesion strength of Ti/TiN multilayer can promote the biocompatibility of TiNi alloy for biomedical applications.

2. Experimental design and methodology

2.1. Substrate material and preparation

The substrate material was Ti-51at%Ni (3 mm thickness), denoted later as a substrate, provided by Stanford Advanced Materials, USA. First, the samples were prepared for coating following the standard methods; grinding using SiC sandpapers from grit no. 180 to 4000 under stream of water. This is followed by polishing to a mirror-like surface via a polishing cloth wetted with colloidal alumina suspension. Then, the surface roughness of the substrates was measured by surface profilometer "SJ-310 Mitutoyo, Japan" to obtain average of roughness below 0.1 μm. This sample preparation assists in achieving better deposition of sputtered materials [48]. The substrates were further cleaned with acetone in ultrasonic bath for 5 min at 40 °C, followed by ethanol, distilled water, and then dried in ambient atmosphere. The cleaning process was carried out to remove contaminations and increase the surface reactivity to form strong chemical bonds.

2.2. Design of Experiment (DOE)

Taguchi orthogonal array (OA) standard of 9-run matrix has been chosen to predict the optimal conditions for each property as well as analysing the interactions between processing parameters. Each parameter was arranged in an OA matrix of three levels, as outlined in Table 1.

2.3. Deposition of multilayer Ti/TiN

The Ti/TiN coating was deposited on Ti-51at%Ni alloy using PVD magnetron sputtering system. The substrates were placed at 12 cm below the pure Ti (99.99 %) target as shown in Fig. 1. First, the chamber was vacuumed down to a base pressure of 2.85×10^{-5} Torr, then argon gas was flown into the chamber to reach a constant pressure of 4.5×10^{-3} Torr. After that, the substrates were heated gradually to the required temperatures according to the OA. Ti interlayer initial deposition was carried out by sputtering the Ti-target for 60 min, followed by pumping a mixed N_2 and Ar atmosphere for 240 min to deposit TiN layer. A three replicates of samples group was synthesized to ensure the reproducibility of samples.

After the completion of the deposition process, the chamber was cooled down to room temperature, then the samples were removed from the substrate holder for further characterization.

2.4. Characterization of Ti/TiN coating on Ti-51at%Ni

The samples surface and cross-section, elemental composition, and the coating thickness were investigated by using FESEM/EDX (ZEISS SIGMA 300 V P Microscopy). The crystal structure and phases present in the Ti/TiN coating were detected using XRD (Rigaku Smart Lab X-Diffraction) using a CuK$_{\alpha 1}$ (α = 1.5406 Å, 40 kV and 30 mA) X-ray source

Table 1
Orthogonal array for experimental runs.

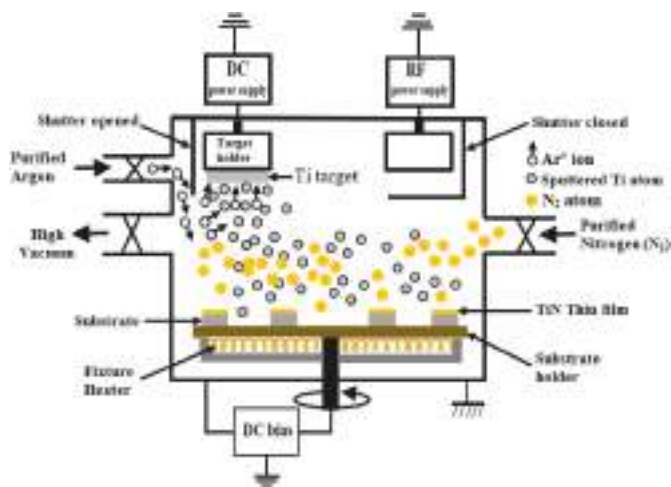| Exp. No.	Parameters and levels			
	Power, W (A)	Temperature, °C (B)	Bias, V (C)	Nitrogen flow rate, sccm (D)
1	300	100	50	5
2	300	150	75	5
3	300	200	100	7
4	370	100	75	7
5	370	150	100	5
6	370	200	50	6
7	440	100	100	6
8	440	150	50	7
9	440	200	75	5

Fig. 1. DC magnetron sputtering device schematic diagram used in the experiment.

radiation. Scanning angle (2θ) from 30° to 90° with a step of 0.10° and grazing angle of 1°.

The hardness test was conducted using a Vickers's Microhardness tester (Shimadzu, HMV-2 Series). The test load was set to 98.07 mN and the dwell time was 5 s. At least three measurements at different locations per sample were taken, and the average values were recorded.

The adhesion of the deposited layer was assessed by scratch test. The critical load (L_{c2}) was determined which indicates the adhesive failure point. The test was conducted using a scratch test machine (Micro Material Nano test, Wrexham, UK) with 25 μm sphero-conical diamond indenter. The test mode was a horizontal scratch with a single pass. A maximum load of 3000 mN, scanning length of 1000 μm and a loading rate of 3 mN s^{-1} were applied on the coating. The lower critical load (L_c) at the start of coating failure is regarded as the smallest load at which significant damage begins, or as the coefficient of friction rises rapidly. The coating failure was further verified by comparing a depth-distance graph with a scratch micrograph obtained by an optical microscope (Olympus BX 61). Hardness and scratch measurements were repeated three times for each sample to ensure the repeatability and reliability of the experiments.

2.5. Taguchi optimization

Taguchi approach uses the signal-to-noise (S/N) ratio as the quality characteristic of the choice [49]. The characteristics of S/N ratio can be divided into three categories when the characteristic is continuous: Nominal is the best, Smaller the better characteristics, or larger the better characteristic. In this research larger the better characteristic category is selected to optimize the process parameters using Eq. (1).

$$S\left/N = -10\ log\frac{1}{n}\left(\sum\frac{1}{y^2}\right)\right. \tag{1}$$

Where (n) is the number of observations, and (y) is the observed data. The obtained process parameters combination was used for confirmation test.

3. Results and discussion

3.1. Hardness and scratch force measurements

The hardness of as-received Ti-51at%Ni was 184 ± 47 HV0.01. The initial multilayer Ti/TiN coating on substrate before optimization was performed based on the OA L9 (3^4) as shown in Table 1. The average hardness and scratch force of the coating were 332 ± 55 HV0.01 and

2709 ± 855 mN respectively showing significant increase in hardness. Table 2 lists the measured hardness, the scratch force, the coating thickness and the corresponding calculated (S/N) ratio using "larger-the-better" quality characteristics method as given in Eq. (1).

As illustrated in Fig. 2, the results of the test showed cohesive failure (L_{C1}) and adhesive failure at the distance of 679.98 μm with critical load (L_{C2}) of 2417 mN, sample **S9**. The failure of the coating was detected by matching the micrograph's critical load to the onset of the coating failure. The critical load is detected when the sudden change in the depth profile matched the delamination of the coating, as shown in the optical image, Fig. 2. A graph of the depth-distance is compared with a micrograph of the scratch track. The drawn line indicates the change of the graph that matches the starting of the coating failure.

The experimental results for hardness test, critical load, coating thickness and their corresponding S/N ratio shown in Table 2 were achieved by using different combination of deposition parameters for each sample, starting from sample1(S1) to sample 9 (S9). The combination of deposition parameters used in S4 for example, is quite different from the parameters used in S8. Therefore, the cohesive failure Lc1 and critical load Lc2 (Adhesive failure) of S4 is treated separately from the Lc1 and Lc2 of S8. The authors used one sample (S9) as shown in Fig. 2, out of the 9 samples used for the experiment. The Lc1 and Lc2 of any sample are peculiar to each individual sample and cannot be compared to other samples because our concern is to find the adhesion strength of each sample that revealed the failure of the TiN coating within itself, known as cohesive failure (Lc1), and failure between the TiN coating and the substrate known as adhesive failure (Lc2) of that particular sample.

In Table 3, the expression "low and high" shows the combination of parameters that gives the lowest and the highest value of coating thickness, critical load, and hardness of the Ti/TiN coating. In this regard, the highest value, which is of interest, is compared with the lowest value to determine the most common parameters that contributed to the coating's highest values.

The experiments showed that nitrogen flow rate at 5 sscm gave the highest values for the coating thickness, hardness and scratch force. However, the effect of each parameter at different factor levels was further evaluated using a (S/N) ratio response analysis to identify a combination of process parameters that are significant in the optimization process.

3.2. Signal-to-noise analysis

After running the experiments, the next step was to conduct data analysis using a S/N ratio to optimize the parameters and determine which process parameters were significant in the optimization process. The signal minimized the variability of factors to S/N ratio and then reduced the variation by optimizing their combined setting [50]. The

Table 2
Experimental results for hardness test, critical load, coating thickness and their corresponding S/N ratio.

| No.	Hardness, HV0.01	Critical load, mN	Coating thickness, μm	S/N Ratio	
				Hardness	Critical load
				S/N(η)	S/N(η)
S1	339 ± 19	2989 ± 78	2.10 ± 0.82	50.5754	69.5105
S2	371 ± 45	1694 ± 13	1.40 ± 0.14	51.2214	64.5783
S3	316 ± 31	1947 ± 37	1.60 ± 0.11	49.7499	65.7873
S4	370 ± 40	3693 ± 98	2.50 ± 0.14	51.2617	71.3476
S5	395 ± 28	3998 ± 91	2.39 ± 0.19	51.8489	72.0369
S6	315 ± 43	3319 ± 39	3.34 ± 0.34	49.8436	70.4201
S7	278 ± 21	1674 ± 51	1.33 ± 0.12	48.7898	64.4751
S8	289 ± 25	2648 ± 57	1.28 ± 0.16	49.1663	68.4584
S9	318 ± 12	2417 ± 42	2.20 ± 0.32	50.0471	67.6655
Average 332 ± 55 2709 ± 855				**50.2782**	**68.2533**
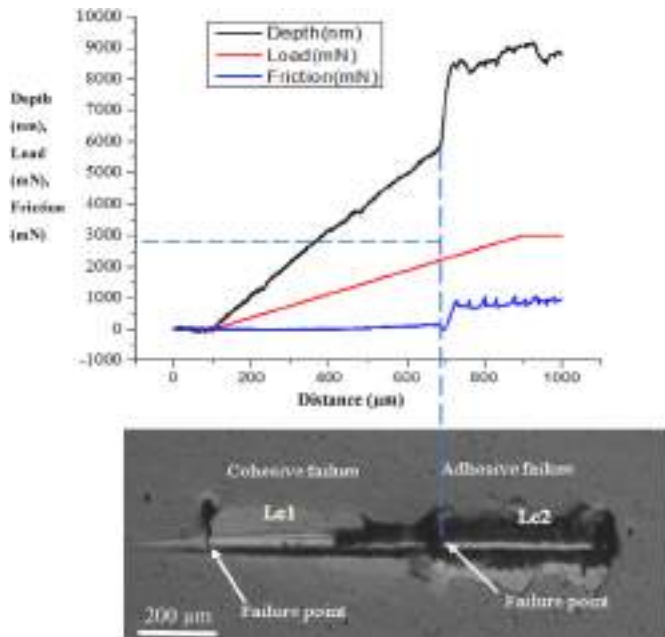
Fig. 2. Optical microscope image for the scratch line.

Table 3
Combination of process parameters during the coating process.

Parameter	Coating thickness		Scratch force		Hardness	
	Low	High	Low	High	Low	High
Power (W)	440	370	300	440	300	440
Temperature (°C)	100	200	200	150	200	150
Bias voltage (V)	75	75	100	100	100	100
N_2 Flow rate (sccm)	7	5	7	5	7	5
Experiment run No.	8	6	7	5	7	5

S/N response value of each level measured data for critical load and hardness were plotted in Figs. 3 and 4, respectively.

The more deflected graphs from horizontal axis, the higher their ranks which means higher significant parameter. From Fig. 3, The DC power (factor A) is more deflected than other parameters, and it is therefore regarded as the most significant, this is followed by N_2 flow rate (factor D), bias voltage (factor C) and lastly temperature (factor B). Therefore, the combination of process parameters with the highest S/N on each factorial level such as DC power (A2), N_2 flow rate (D1), bias voltage (C1), and temperature (B1) are taken as the optimal parameters

to obtain higher scratch force – which means improved adhesion strength - and are denoted as A2D1C1B1 (370 W, 5 sccm, 50 V and 100 °C).

Similarly, Fig. 4 shows that DC power (factor A) is ranked number 1 as the most significant parameter followed by bias voltage (factor C), N_2 flow rate (factor D) and temperature (factor B), respectively. The optimum combination of process parameters to achieve the required high surface hardness are, therefore, DC power (A2), bias voltage (C2), nitrogen flow rate (D1), temperature (B2) and are denoted as A2C2D1B2 (370 W, 75 V, 5 sccm and 150 °C). Table 4 presents the confirmation test of optimal parameters combinations to validate the results of parameters obtained.

A higher N_2 flow rate causes an increase in chamber pressure, which leads to a rise in sputtering rate as the ionised atoms increase in the plasma [51,52]. On the contrary, the likelihood of collision between nitrogen atoms and sputtered particles on their way to the substrate increases due to the high quantity of gas atoms [53]. In that case, the free movement of nitrogen gas is hindered due to the collision and eventually leads to a low deposition rate. However, the low nitrogen flow rate gave a higher deposition rate due to the decrease in chamber pressure, which allowed free movement of atoms and sputtered particles to be deposited on the substrate. Figs. 3 and 4 show that the nitrogen flow rate at 5 sccm contributes more to the scratch force and surface hardness. When high chamber pressures are used, the process reduces the sputtered atoms energy and enables the substrate to have its surface covered with positively charged particles [54].

If the pressure remains constant with increasing the power, the ion concentration increases and hence the rate of sputtering increases. When the power is increased further, the rate of sputtering decreases due to back diffusion, as shown in Figs. 3 and 4. As the power increased to 300 W and 370 W, more energy is gained by the electrically charged ionised and sputtered particles. This increased the sputtering rate and thus increased the scratch force and hardness. Alternatively, when the power increases further to 440 W, the collision between chamber particles and sputtered particles increases. Consequently, a substantial drop in the sputtering rate occurs due to high power sputtering which eventually led to a decrease in the scratch force and surface hardness.

The effect of temperature on the scratch force and surface hardness is relatively insignificant compared to other parameters, as indicated in Figs. 3 and 4. The scratch force of the coating at 100 °C is higher compared to when the substrate is coated at 150 °C and 200 °C, as shown in Fig. 3, which is regarded to low gas pressure at high temperatures [55]. Although the hardness improved when the temperature is raised from 100 °C to 150 °C, the hardness somehow reduced at 200 °C due to a slower movement of atoms.

The experiments indicated that the application of bias voltage at 50 V increases the scratch force. However, the scratch force decreases with
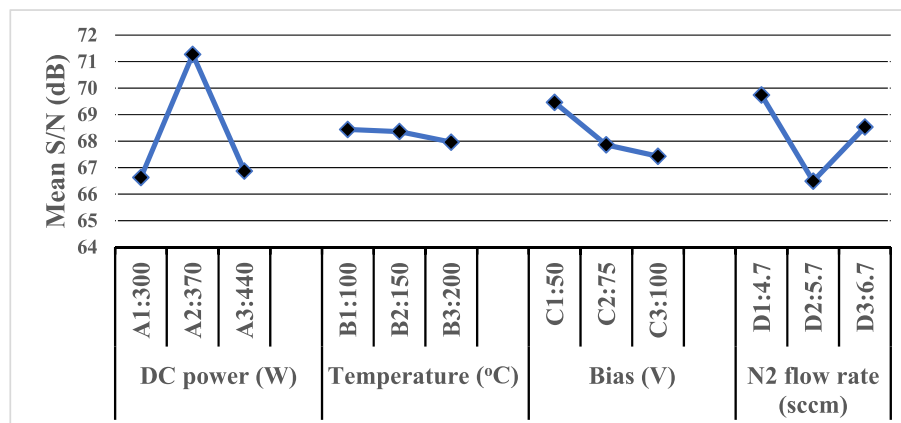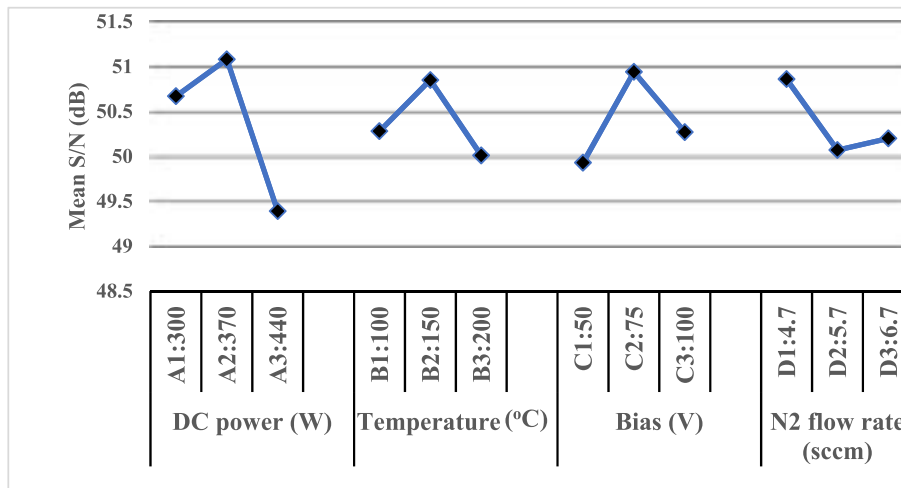

Fig. 3. Scratch force S/N response.

Fig. 4. Surface hardness S/N response.

Table 4
Optimum parameters for confirmation test.

	Power (W)	Temperature (°C)	Bias Voltage (V)	N$_2$ (sccm)
	A	B	C	D
Ti-51at% Ni	**Surface hardness**			
	S/N 51.08	50.85	50.94	50.86
	VP[a] 370	150	75	5
	Scratch force			
	S/N 71.27	68.44	69.46	69.74
	VP[a] 370	100	50	5

[a] VP: Variable parameters.

the increase of bias voltage from 50 V to 75 V and 100 V due to the defects in growing film which is regarded to high-energy bombardment [56]. The hardness of TiN coating increased with an increase in bias voltage from 50 V to 75 V due to re-sputtering of loosely bound atoms [57], while decreased from 75 V to 100 V. As shown in Fig. 4, A2C2D1B2 are the combination of significant parameters to achieve improved surface hardness.

3.3. Confirmation test

A confirmation test was performed to establish the validity and reliability of the combination of parameters for both scratch force and surface hardness. The findings are estimated by the reduced equation of S/N ratio predicted value [50,58]:

$$\bar{\mu} = \overline{A2} + \overline{B2} + \overline{C2} + \overline{D1} - \overline{3Y} \tag{4}$$

$$\bar{\mu} = \overline{A2} + \overline{B1} + \overline{C1} + \overline{D1} - \overline{3Y} \tag{5}$$

Where $(\bar{\mu})$ is the predicted S/N ratio; $(\overline{A2}, \overline{B2}, \overline{C2}$ and $\overline{D1})$ and $(\overline{A2}, \overline{B1}, \overline{C1}$ and $\overline{D1})$ are the average value of optimum surface hardness and scratch force, respectively. $(\overline{Y})$ is the average value of the overall surface hardness and scratch force.

The $(\bar{\mu})$ gave the values 74.16 dB and 52.59 dB for scratch force and hardness, respectively. The mean S/N ratio value from the confirmation test was 69.54 dB and 50.71 dB for scratch force and hardness, respectively. The results show that the confirmation test is in good agreement with the predicted ones.

Furthermore, the optimum parameters determined were used to deposit a new Ti/TiN coating on Ti-51at%Ni. It was noted that the hardness and scratch force recorded after the confirmation test were 344 ± 16 HV0.01 and 3000 ± 191 mN, respectively. The final results showed that the optimization increased the average hardness from 322 ± 55 to

344 ± 16 HV0.01 (6.83 %), and the scratch force increased from 2709 mN to 3000 mN with 10.74 % improvement.

3.4. Characterization of the coated samples

The phases and crystallinity of the multilayer Ti/TiN coating at two conditions (370 W, 75 V, 5 sccm, 150 °C and 370 W, 50 V, 5 sccm, 100 °C) were revealed by XRD in Fig. 5. These conditions were selected as they showed the best response (hardness and scratch force). The results of the analysis revealed a homogeneous coating by the detection of TiN peaks intensities at 36.61° (111), 42.53° (200), 61.90° (220), 74.00° (311) and 77.31° (222). This agrees with the result of the study carried out previously [59]. It is obvious that the crystal planes are of face centred cubic (FCC) with only TiN peaks present in the coating with space group (225) (Fm-3m and lattice parameters a = b = c = 4.245, ICDD Card No. 01-087-0626).

The mixed diffraction peaks exhibited by TiN showed different film intensities of various orientations. Generally, there are three main types of preferred orientations, such as (111), (200) and (220) when TiN is deposited using PVD methods [60,61]. The (111) preferred orientation of TiN films is usually associated with the lowest strain energy, (200) preferred orientation is attributed to the lowest surface energy [62], and (220) occurs due to the lowest stopping energy which becomes dominant only when the deposited ion energy is high enough [43,63].
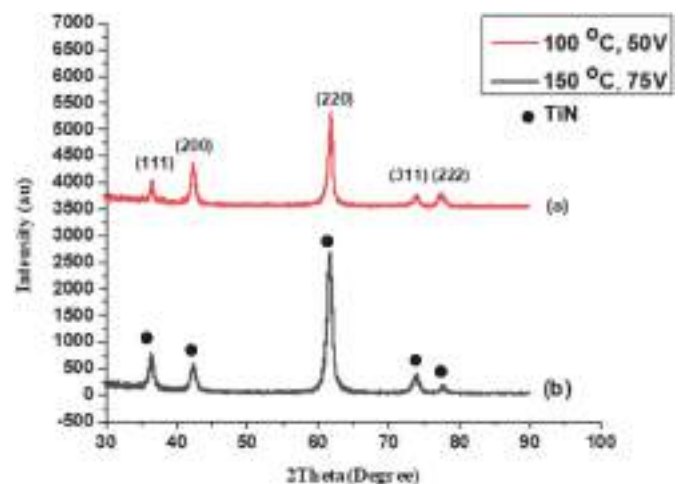

Fig. 5. The XRD patterns of Ti/TiN coatings: (a) 370 W, 75 V, 5 sccm, 150 °C, (b) 370 W, 50 V, 5 sccm, 100 °C.

As shown in Fig. (5) and (220) is the dominant preferred orientation observed, which indicates that the ion energy is sufficiently high. The relatively low peak intensity of (111) plane in Fig. 5 (a) is due to low temperature (100 °C) and bias voltage of (50 V) when compared to the higher peak intensity of (111) plane at a temperature of 150 °C and bias voltage of 75 V, Fig. 5 (b). This can be regarded to the higher substrate temperature, in this case, that has a low gas pressure effect due to the free movement of high-energy atoms with high mobility on the surface of the substrate. The low peak intensity of (200) plane, Fig. 5 (b), corresponds to the lowest surface free energy occurred due to high adatom mobility that is attributable to the increase in temperature and bias voltage [64]. The peak intensity of (222) plane decreases with the increase in temperature and bias voltage, which signifies that it follows the same trend as (200) plane while the peak intensity of (311) increases with the increase in temperature and bias voltage as (111) and (220) planes.

The FESEM imaging of the surface morphology of Ti/TiN coated samples is shown in Fig. 6. It revealed that the surfaces of the coated samples consist of a similar pyramid-like structure with different crystal grain size as shown in Fig. 6 (a) and 6 (b), respectively. The pyramid-like shape is due to the preferred growth along the (220) plane of the coatings [65] as illustrated in the XRD analysis.

The surface morphology of each coating clearly shows that each grain size is distributed uniformly, and the grains are packed closely without any noticeable pores, Fig. 6. The difference in the grain size could be attributed to the difference in the deposition parameters such as temperature and bias voltage. As observed in Fig. 5 (a), the preferred (220) peaks become more intense as the bias voltage and temperature increased from 100 °C to 50 V to 150 °C and 75 V, respectively. The increase in bias voltage triggered the bombardment of energetic ions on the growing films continually, and the increase in temperature ensures the mobility of the adatoms to the surface of the coating to form crystalline films. As the crystallinity improved, the crystal grain size becomes larger under the same magnification (*x*2500), Fig. 6.

The number of grains and their distributions was established using Image analysis software (ImageJ). In Fig. 7, the results indicated that the crystallite grain size of TiN deposited at 50 V and 100 °C appeared smaller and more in counts, while the one deposited at 75 V and 150 °C appeared bigger and less in counts which conforms with the earlier discussions.

Ti/TiN coating (100 °C, 50 V and 150 °C, 75 V) cross-sectional views are shown in Fig. 8 (a) and 8 (b), respectively. The deposition rate in the samples with lower deposition temperatures and Bias is higher due to the influence of other parameters such as N_2 flow rate, power and pressure. The coating layers exhibited a dense structure without any recognized cracks or voids between the substrate and the coating. The cross-sectional measurement of the sample using FESEM showed that the different coating conditions produced different thicknesses. It is clearly appeared the doping of nitrogen into the Ti-interlayer according to the EDX line scan, Fig. 8 (c). As the level of nitrogen doping increases, there is a general trend that the hardness of Ti-interlayer increases [42, 66,67].

The Ti-interlayer becomes stronger with nitrogen gas and can provide increased support for the TiN layer, resulting in increased scratch force. The increase in the scratch force can be attributed to the increased strength of Ti-interlayer influenced by nitrogen as well as due to the decomposition of the native oxide film present on the surface of the substrate caused by the acquired oxygen on Ti-interlayer. However, the further increase in nitrogen content leads to the observed decrease in scratch force, shown in Fig. 3, as the interlayer becomes too brittle to accommodate the interfacial stresses.

4. Conclusion

Ti/TiN was successfully deposited on Ti-51at%Ni substrate by DC magnetron sputtering method. The deposition was conducted at three levels of selected process parameters: DC power (300, 370, 440 W), temperature (100, 150, 200 °C), substrate bias voltage (50, 75, 100 V) and nitrogen flow rate (5, 6, 7 sccm).

Via the formula provided by Taguchi method, nine experiments were conducted to determine the parameters combination for optimum adhesion strength (expressed by scratch force) and hardness of the coating layer. The confirmation tests showed that scratch force (3000 ± 191 mN) was maximum at 370 W, 100 °C, 50 V and 5 sccm for DC power, temperature, substrate bias voltage and nitrogen flow rate, respectively. Meanwhile optimum hardness (344 ± 16 HV0.01) could be best presented at 370 W, 150 °C, 75 V and 5 sccm for DC power, temperature, substrate bias voltage and nitrogen flow rate, respectively. The multilayer Ti/TiN thin films deposited using the optimum conditions indicated the scratch force was improved by 10.74 %, and the hardness was improved by 6.83 % compared to the average values of L9 samples. The combination of parameters leads the way in achieving best properties of potential biomaterials for extended research.
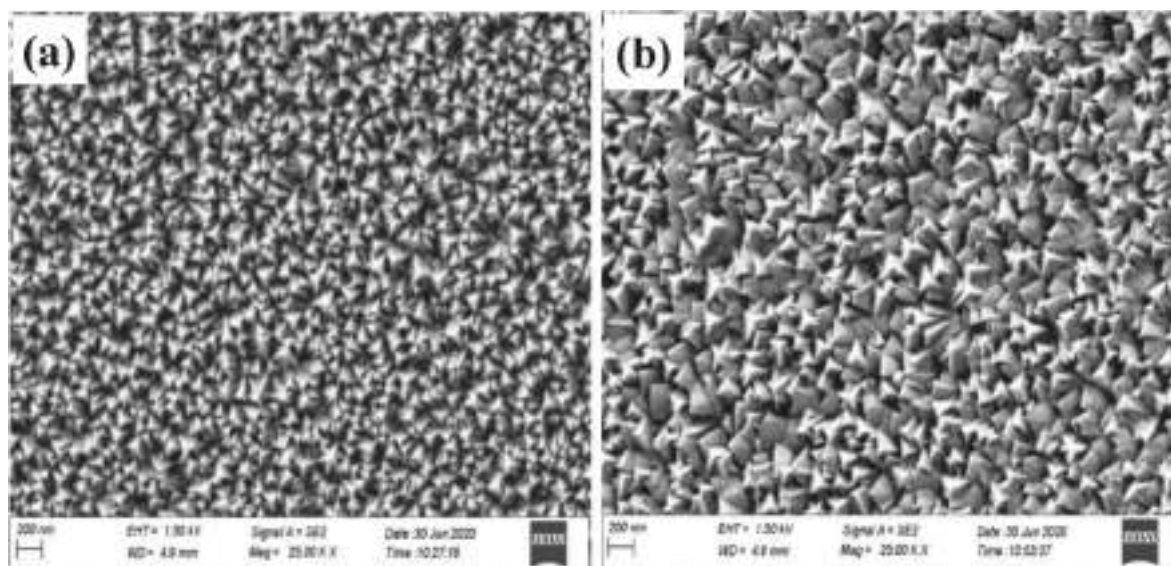

Fig. 6. The FESEM surface morphology of Ti/TiN coating at: (a) 50 V and 100 °C, (b) 75 V and 150 °C.
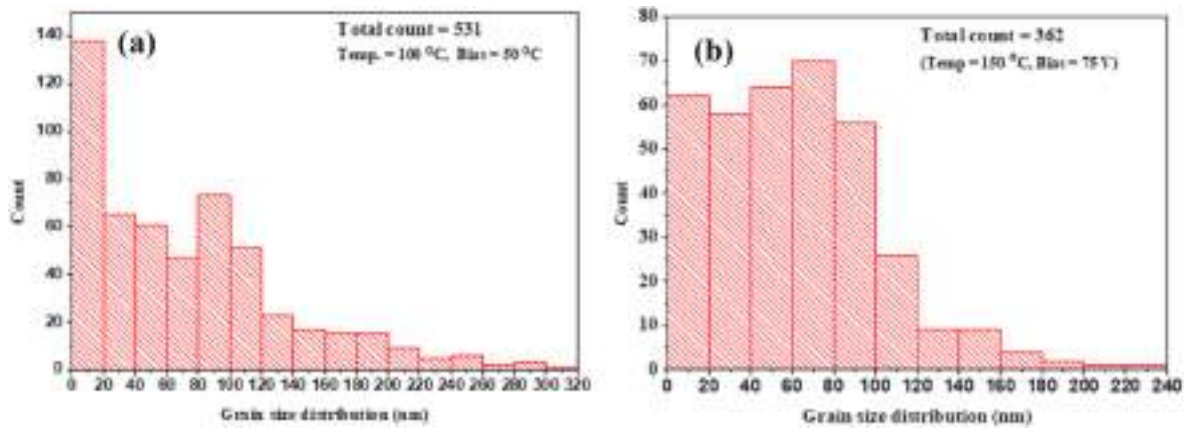
Fig. 7. Grain size distribution of TiN coating at (a) 100 °C, 50 V (b) 150 °C, 75 V.
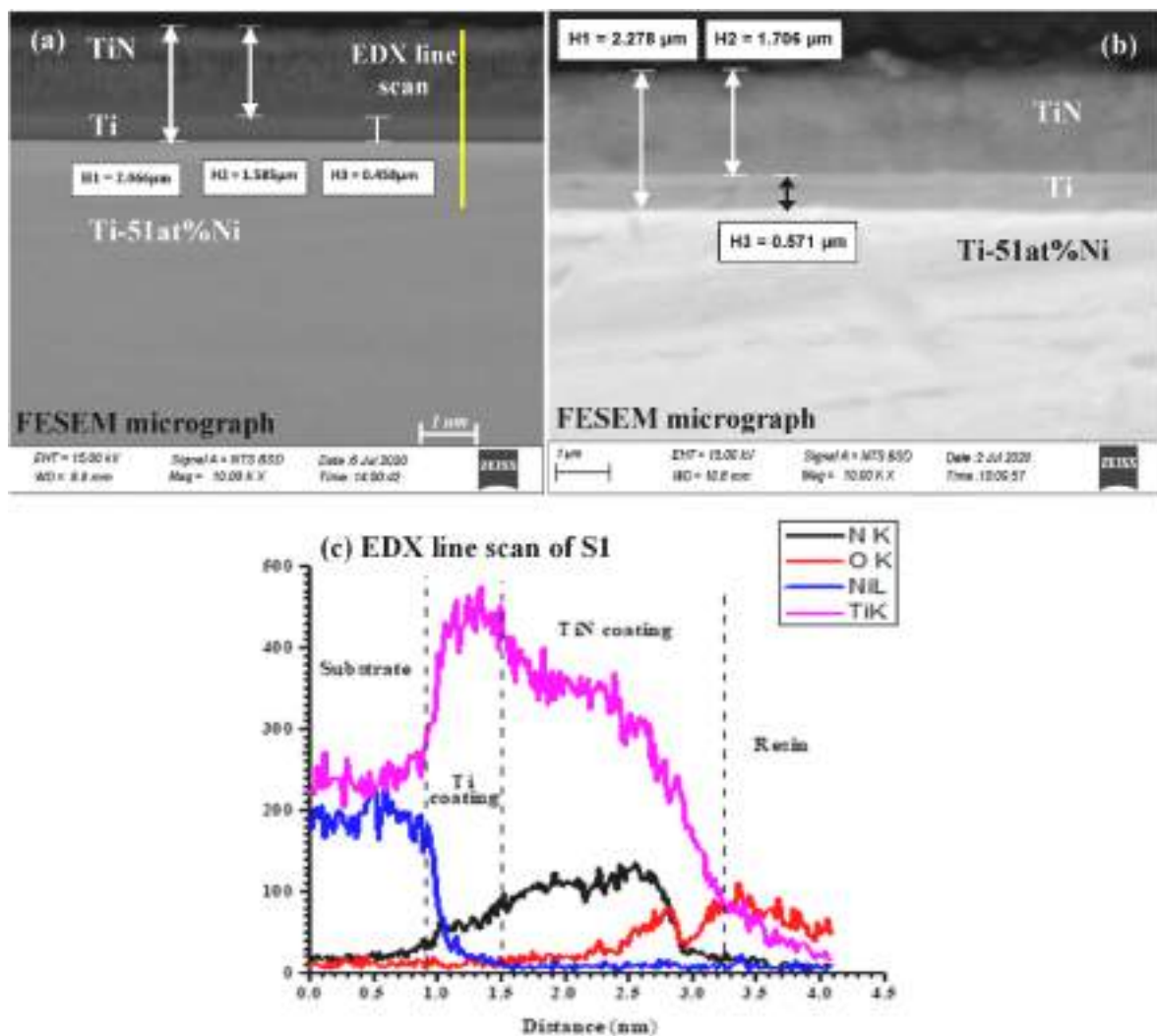

Fig. 8. Cross-sectional FESEM micrograph of the Ti/TiN coating at: (a) S1 (b) S2 (c) EDX line scan along the cross-section of S1.

CRediT authorship contribution statement

Ishiaka Shaibu Arudi: Conceptualization, Methodology, Investigation, Data curation, Formal analysis, Writing – original draft. **Esah Hamzah:** Resources, Supervision, Funding acquisition, Project administration, Validation M Azizi Mat Yajid: Supervising. Abdul Razak Bushroa**:** Supervision, Methodology, Resources, Writing – review & editing. **Shadi M. Munshi:** Funding acquisition, Writing – review & editing. **M. S. Al-Ashhab:** Writing – review & editing. **M. Zakaria Ibrahim:** Writing – review & editing.

Declaration of competing interest

The authors declare that they have no known competing financial interests or personal relationships that could have appeared to influence the work reported in this paper.

Acknowledgement

References

[1] Zhu J, Zeng Q, Fu T. An updated review on TiNi alloy for biomedical applications. Corrosion Reviews 2019;vol. 37:539–52.

[2] Jin S, Zhang Y, Wang Q, Zhang D, Zhang S. Influence of TiN coating on the biocompatibility of medical NiTi alloy. Colloids Surf B Biointerfaces 2013;101:343.–9.

[3] Tang G, Ho JKL, Dong G, Hua M. Fabrication self-recovery bulge textures on TiNi shape memory alloy and its tribological properties in lubricated sliding. Tribol Int 2016;96:11–22.

[4] Ibrahim MK, Saud SN, Hamzah E, Nazim EM. In Vitro Microstructure, Shape Memory, Corrosion, and Biocompatibility Characteristics of Porous Ti-51 at.%Ni-xSn Shape Memory Alloys. Metallogr Microstr Anal 2022;11:150. 7.

[5] Saedi S, Saghaian SE, Jahadakbar A, Moghaddam NS, Andani MT, Saghaian SM, Lu YC, Elahinia M, Karaca HE. Shape memory response of porous NiTi shape memory alloys fabricated by selective laser melting. J Mater Sci Mater Med 2018; 29:1. –12.

[6] Zhu J, Zeng Q, Fu T. An updated review on TiNi alloy for biomedical applications *Corrosion Reviews*, vol. 37; 2019. p. 539–52.

[7] Zhang Y, Zhang Z, Xie Y, Wang S, Qiu Q, Zhou Y, Zeng G. Toxicity of nickel ions and comprehensive analysis of nickel ion-associated gene expression profiles in THP-1 cells. Mol Med Rep 2015;12:3273–8.

[8] McNamara K, Beloshapkin S, Hossain KM, Dhoubhadel MS, Tofail SAM. Tantalum coating inhibits Ni-migration from titanium out-diffusion in NiTi shape memory biomedical alloy. Appl Surf Sci 2021;535.

[9] Bernard SA, Balla VK, Davies NM, Bose S, Bandyopadhyay A. Bone cell–materials interactions and Ni ion release of anodized equiatomic NiTi alloy. Acta Biomater 2011;7:1902. 12.

[10] Tran PA, Sarker A, Tran N, Jeffery C, Rifai A, Fox K. Coatings on metallic implants for biomedical applications. Metallic Biomater Proces Med Device Manufac 2020: 359–85. Elsevier.

[11] Meisner LL, Markov AB, Rotshtein VP, Ozur GE, Meisner SN, Yakovlev EV, Semin VO, Mironov YP, Poletika TM, Girsova SL. Microstructural characterization of Ti-Ta-based surface alloy fabricated on TiNi SMA by additive pulsed electron-beam melting of film/substrate system. J Alloys Compd 2018;730:376–85.

[12] Prasad K, Bazaka O, Chua M, Rochford M, Fedrick L, Spoor J, Symes R, Tieppo M, Collins C, Cao A, Id D M, Ostrikov KK, Bazaka K. Metallic biomaterials. Current Challenges and Opportunities Materials 2017;10:1–33.

[13] Meisner LL, Markov AB, Rotshtein VP, Ozur GE, Meisner SN, Yakovlev EV, Semin VO, Mironov YP, Poletika TM, Girsova SL. Microstructural characterization of Ti-Ta-based surface alloy fabricated on TiNi SMA by additive pulsed electron-beam melting of film/substrate system. J Alloys Compd 2018;730:376–85.

[14] Ibrahim MZ, Sarhan AAD, Yusuf F, Hamdi M. Biomedical materials and techniques to improve the tribological, mechanical and biomedical properties of orthopedic implants – a review article. J Alloys Compd 2017;714:636–67.

[15] Jin S, Zhang Y, Wang Q, Zhang D, Zhang S. Influence of TiN coating on the biocompatibility of medical NiTi alloy. Colloids Surf B Biointerfaces 2013;101:343. –9.

[16] Abubakar T, Rahman M, Dowling DP, Stokes J, Hashmi MSJ. Adhesion performance of TiN coating with amorphous NiTi alloy interlayer onto 316L stainless biosteel deposited by sputtering process. Surf Eng 2010;26:499–505.

[17] Luo Y, Ge S. Fretting wear behavior of nitrogen ion implanted titanium alloys in bovine serum lubrication. Tribol Int 2009;42:1373–9.

[18] Filip P, Kneissl AC, Mazanec K. Physics of hydroxyapatite plasma coatings on TiNi shape memory materials. Mater Sci Engin 1997;234(236):422. 5.

[19] Ashuri M, Moztarzadeh F, Nezafati N, Ansari Hamedani A, Tahriri M. Development of a composite based on hydroxyapatite and magnesium and zinc-containing sol–gel-derived bioactive glass for bone substitute applications. Mater Sci Engin 2012;C 32(2330):9.

[20] Pourhashem S, Afshar A. Double layer bioglass-silica coatings on 316L stainless steel by sol-gel method. Ceram Int 2014;40:993–1000.

[21] Balla VK, Xue W, Bose S, Bandyopadhyay A. Laser-assisted Zr/ZrO2 coating on Ti for load-bearing implants. Acta Biomater 2009;5:2800–9.

[22] Mansur MR, Wang J, Berndt CC, Rakib M, Wang J, Berndt CC. Microstructure, composition and hardness of laser-assisted hydroxyapatite and Ti-6Al-4V composite coatings. Surf Coat Technol 2013;232:482–8.

[23] Vikulova ES, Karakovskaya KI, Koretskaya TP, Korolkov I v, Chepeleva E v, Asanov IP, Tsygankova AR, Maksimovskii EA, Marchenko ES, Lantsukhay YA, Zheravin AA, Morozova NB. MOCVD of noble metal film materials for medical implants: microstructure and biocompatibility of Ir and Au/Ir coatings on TiNi *COATINGS* 11. 2021.

[24] Shah A, Izman S, Hassan MA. Influence of nitrogen flow rate in reducing tin microdroplets on biomedical TI-13ZR-13NB alloy. J Teknol 2016;78.

[25] Ghufran M, Uddin GM, Khan AA, Hussein H, Khurshid K, Arafat SM. Comparative experimental investigation of mechanical properties and adhesion of low temperature PVD coated TiO2 thin films. Lecture Notes in Mechan Eng 2019; 451–60.

[26] Łapaj Ł, Wendland J, Markuszewski J, Mróz A, Wiśniewski T. Retrieval analysis of titanium nitride (TiN) coated prosthetic femoral heads articulating with polyethylene. J Mech Behav Biomed Mater 2016;55:127–39.

[27] van Hove RP, Sierevelt IN, van Royen BJ, Nolte PA. Titanium-nitride coating of orthopaedic implants: a review of the literature. BioMed Res Int 2015;(2015).

[28] Othman MF, Bushroa AR, Abdullah WNR. Evaluation techniques and improvements of adhesion strength for TiN coating in tool applications: a review. J Adhes Sci Technol 2015;29:569–91.

[29] de Langkruis van, Hosson D, Sabooni S, Galinmoghaddam E, Ahmadi M, Westerwaal R, van de Langkruis J, Zoestbergen E, De Hosson Jt, Pei Y. Microstructure and adhesion strength quantification of PVD bi-layered ZnMg-Zn coatings on DP800 steel. Surf Coat Technol 2019;359:227–38.

[30] Berbecaru C, Stan GE, Pina S, Tulyaganov DU, Ferreira JMF. The bioactivity mechanism of magnetron sputtered bioglass thin films. Appl Surf Sci 2012;258: 9840–8.

[31] Chien CS, Liu CW, Kuo TY, Wu CC, Hong TF. Bioactivity of fluorapatite/alumina composite coatings deposited on Ti6Al4V substrates by laser cladding. Appl Phys A 2016;122:303.

[32] Comesaña R, Quintero F, Lusquiños F, Pascual MJ, Boutinguiza M, Durán A, Pou J. Laser cladding of bioactive glass coatings Acta. Biomaterials 2010;6:953–61.

[33] Aragón-Duarte MC, Nevarez-Rascón A, Esparza-Ponce HE, Nevarez-Rascón MM, Talamantes RP, Ornelas C, Mendez-Nonell J, González-Hernández J, Yacamán MJ, Hurtado-Macías A. Nanomechanical properties of zirconia- yttria and alumina zirconia- yttria biomedical ceramics, subjected to low temperature aging. Ceram Int 2017;43:3931–9.

[34] Schiltz J, Rosenberger A, Render T, Gatrell BA, Qu H, Steiner C, McGinn P, Schmid S. Wear of structural oxide ceramics produced through additive manufacturing. Procedia Manuf 2019;34:780. 8.

[35] Guazzato M, Albakry M, Ringer SP, Swain MV. Strength, fracture toughness and microstructure of a selection of all-ceramic materials. Part II. Zirconia-based dental ceramics. Dental Materials 2004;20:449–56.

[36] Kiechle S, Liebermann A, Mast G, Heitzer M, Möhlhenrich SC, Hölzle F, Kniha H, Kniha K. Evaluation of one-piece zirconia dental implants: an 8-year follow-up study. Clin Oral Invest 2023;27.

[37] Wu W-Y, Chan M-Y, Hsu Y-H, Chen G-Z, Liao S-C, Lee C-H, Lui P-W. Bioapplication of TiN thin films deposited using high power impulse magnetron sputtering. Surf Coat Technol 2019;362:167–75.

[38] Ali R, Sebastiani M, Bemporad E. Influence of Ti–TiN multilayer PVD-coatings design on residual stresses and adhesion. Mater Des 2015;75:47–56.

[39] Todt J, Pitonak R, Köpf A, Weißenbacher R, Sartory B, Burghammer M, Daniel R, Schöberl T, Keckes J. Superior oxidation resistance, mechanical properties and residual stresses of an Al-rich nanolamellar Ti0. 05Al0. 95N coating prepared by CVD. Surf Coat Technol 2014;258:1119–27.

[40] Jiang CL, Zhu HL, Shin KS, Tang YB. Influence of titanium interlayer thickness distribution on mechanical properties of Ti/TiN multilayer coatings. Thin Solid Films 2017;632:97–105.

[41] Yanfeng W, Zhengxian L, Haonan W, Jihong D, Changwei Z. Effect of multilayered structure on properties of Ti/TiN coating. Rare Metal Mater Engin 2017;vol. 46: 1219–24.

[42] Baigonakova GA, Marchenko ES, Yasenchuk YF, Kokorev O v, Vorozhtsov AB, Kulbakin DE. Microstructural characterization, wettability and cytocompatibility of gradient coatings synthesized by gas nitriding of three-layer Ti/Ni/Ti nanolaminates magnetron sputtered on the TiNi substrate. Surf Coat Technol 2022; 436.

[43] Li HT, Sun PF, Cheng DH, Liu ZM. Effects of deposition temperature on structure, residual stress and corrosion behavior of Cr/TiN/Ti/TiN films. Ceram Int 2021;47: 34909–17.

[44] Ali R, Sebastiani M, Bemporad E. Influence of Ti–TiN multilayer PVD-coatings design on residual stresses and adhesion. Mater Des 2015;75:47–56.

[45] Zalnezhad E, Sarhan AAD, Hamdi M. Optimizing the PVD TiN thin film coating's parameters on aerospace AL7075-T6 alloy for higher coating hardness and adhesion with better tribological properties of the coating surface. Int J Adv Des Manuf Technol 2013;64:281–90.

[46] Wu W-Y, Chan M-Y, Hsu Y-H, Chen G-Z, Liao S-C, Lee C-H, Lui P-W. Bioapplication of TiN thin films deposited using high power impulse magnetron sputtering. Surf Coat Technol 2019;362:167–75.

[47] Yang YH, Chen DJ, Wu FB. Microstructure, hardness, and wear resistance of sputtering TaN coating by controlling RF input power. Surf Coat Technol 2016; 303:32–40.

[48] Shah A, Izman S, Ismail SNF, Mas-Ayu H, Daud R. Study on adhesion strength of tin coated biomedical Ti-13Zr-13Nb alloy. J Teknol 2018;80.

[49] Karna SK, Sahai R. An overview on Taguchi method. Int J Engin Mathem Sci 2012; 1:1. –7.

[50] Yu D, Wang C, Cheng X, Zhang F. Optimization of hybrid PVD process of TiAlN coatings by Taguchi method. Appl Surf Sci 2008;255:1865–9.

[51] Kelly PJ, Arnell RD. Magnetron sputtering: a review of recent developments and applications. Vacuum 2000;56:159. 72.

[52] Reichelt K, Jiang X. The preparation of thin films by physical vapour deposition methods. Thin Solid Films 1990;191:91. 126.

[53] Frey H, Kienel G. Dünnschichttechnologie (Thin film technology). VDI-Verlag; 1987 [Düsseldorf (in German)].

[54] Tan CW, Miao J. Optimization of sputtered Cr/Au thin film for diaphragm-based MEMS applications. Thin Solid Films 2009;517:4921. 5.

[55] Thornton JA. High rate thick film growth. Annual Rev Mater Sci 1977;7:239–60.

[56] Gangopadhyay S, Acharya R, Chattopadhyay AK, Paul S. Effect of substrate bias voltage on structural and mechanical properties of pulsed DC magnetron sputtered TiN–MoSx composite coatings. Vacuum 2010;vol. 84:843–50.

[57] Thompson CV. Structure evolution during processing of polycrystalline films. Annual Rev Mater Sci 2000;30:159. 90.

[58] Karna SK, Sahai R. An overview on Taguchi method. Int J Engin Mathem Sci 2012; 1:1. 7.

[59] Shah A, Izman S, Ismail SNF, Mas-Ayu H, Daud R. Study on adhesion strength of tin coated biomedical Ti-13Zr-13Nb alloy. J Teknol 2018;80.

[60] Khojier K, Savaloni H, Shokrai E, Dehghani Z, Dehnavi NZ. Influence of argon gas flow on mechanical and electrical properties of sputtered titanium nitride thin films. J Theoret Appl Phy 2013;7:1–6.

[61] Sun F, Liu XL, Luo SQ, Xiang DD, Ba DC, Lin Z, Song GQ. Duplex treatment of arc plasma nitriding and PVD TiN coating applied to dental implant screws. Surf Coat Technol 2022;439.

[62] Zhang S, Yan F, Yang Y, Yan M, Zhang Y, Guo J, Li H. Effects of sputtering gas on microstructure and tribological properties of titanium nitride films. Appl Surf Sci 2019;488:61–9.

[63] Arshi N, Lu J, Joo YK, Lee CG, Yoon JH, Ahmed F. Study on structural, morphological and electrical properties of sputtered titanium nitride films under different argon gas flow. Mater Chem Phys 2012;134:839–44.

[64] Greene JE, Sundgren J, Hultman L, Petrov I, Bergstrom DB. Development of preferred orientation in polycrystalline TiN layers grown by ultrahigh vacuum reactive magnetron sputtering. Appl Phys Lett 1995;67:2928–30.

[65] Chen JT, Wang J, Zhang F, Zhang GA, Fan XY, Wu ZG, Yan PX. Characterization and temperature controlling property of TiAlN coatings deposited by reactive magnetron co-sputtering. J Alloys Compd 2009;472:91–6.

[66] Chunyan Y, Linhai T, Yinghui W, Shebin W, Tianbao L, Bingshe X. The effect of substrate bias voltages on impact resistance of CrAlN coatings deposited by modified ion beam enhanced magnetron sputtering. Appl Surf Sci 2009;255: 4033–8.

[67] Mubarak A, Hamzah E. Influence of nitrogen gas flow rate on the microstructural and mechanical properties of tin deposited carbon steel synthesized by cae. ASEAN J Sci Technol Dev 2006;23:239–51.